



CrossMark
click for updates

Cite this: *RSC Adv.*, 2017, 7, 1146

Sm³⁺ and Eu³⁺ codoped SrBi₂B₂O₇: a red-emitting phosphor with improved thermal stability†

Liwei Wu,^a Yuxing Bai,^a Li Wu,^{*a} Huan Yi,^a Yongfa Kong,^a Yi Zhang^{*b} and Jingjun Xu^a

The thermal stability of luminescence is very critical for white light-emitting diodes. However, it is a continuous challenge to improve the thermal stability of red phosphors. In this study, Sm³⁺ and Eu³⁺ codoped SrBi₂B₂O₇ was synthesized by a high temperature solid state reaction method. It was found that the thermal stability of the synthesized phosphors was improved as Sm³⁺ was used as the sensitizer for Eu³⁺ doped into SrBi₂B₂O₇. Combined with a local crystal environment study and the first-principles calculations, the origin of the improvement of this thermal stability was studied in detail. The doped Sm³⁺ and Eu³⁺ ions were inclined to occupy Bi(1) (6c) and Bi(2) (6c) sites simultaneously and the crystal structure of the SrBi₂B₂O₇:Sm³⁺, Eu³⁺ was more compact at high temperature than that at room temperature. Thus, the defect formation energy was very low in the Sm³⁺ and Eu³⁺ codoped SrBi₂B₂O₇ phosphor, which is the main reason to improve the thermal stability with Sm³⁺ and Eu³⁺ codoped into SrBi₂B₂O₇. This study provides a new idea for developing a new method to improve the thermal stability of red-emitting phosphors.

Received 14th November 2016
Accepted 20th December 2016

DOI: 10.1039/c6ra26752a

www.rsc.org/advances

1. Introduction

In high-power w-LEDs, when they are working the temperature of the layer deposited on the chip can rise to more than 150 °C because of the thermal effect from the p-n junction and the phosphor layer. Thus, the thermal stability of the phosphor has a great influence on the light output and color rendering index, and it is a vital factor for the application of w-LEDs. At about 150 °C, lots of the phosphors cannot show good thermal stability compared with those kept at room temperature. Up-to-now, some nitrides or oxynitrides have been proved to be good performance red phosphors because of their good thermal stability.^{1,2} However, the synthesis of those phosphors requires a very high nitrogen pressure and high sintering temperature, which often results in much higher production costs. Therefore, it is highly desirable to develop new phosphors, especially red emitting phosphors, with excellent thermal stability and lower cost for warm white-light emission.

As a kind of rare earth ions, Sm³⁺ ions generate intense reddish orange emitting light because it can be excited to its ⁴F_{7/2} energy

level and then relaxed to the ⁴G_{5/2} energy level through the non-radiative transition.³⁻⁵ Eu³⁺ ions have been widely studied as an activator for red light emitting materials due to the ⁵D₀ → ⁷F_J (J = 0, 1, 2, 3, 4) transition of Eu³⁺.⁶⁻⁸ Presently most of used red phosphors are single doped by Sm³⁺ or Eu³⁺, such as Y₂O₃:Eu³⁺,⁹ Y₂O₃:Eu³⁺,¹⁰ BaMoO₄:Sm³⁺,¹¹ SrCaMoO₆:Sm³⁺¹² *et al.* However, the majority of them show limited thermal stability.

As for the low-cost phosphors, rare-earth ions doped borates phosphors is a potential candidate because of their low synthesis temperature and high chemical and physical stability,¹³ such as Ba₂Tb(BO₃)₂Cl:Eu³⁺,¹⁴ and KSr₄(BO₃)₃:Sm³⁺.¹⁵ As Sm³⁺ and Eu³⁺ codoped into hosts, energy transfer from Sm³⁺ to Eu³⁺ can enhance the emission of the Eu³⁺ ions and extend the excitation spectrum. Thus energy transfer between Sm³⁺ and Eu³⁺ is important to adjust the photoluminescence properties. Up to now, this energy transfer has been investigated in some phosphors.¹⁶⁻¹⁸ However, Sm³⁺ and Eu³⁺ codoped into suitable borates material, thus appearing energy transfer, especially improving thermal stability of the phosphor has not been reported to our knowledge.

In this study, SrBi₂B₂O₇ was considered as the host. SrBi₂B₂O₇, synthesized by J. Barbier's group in 2006,¹⁹ is crystallized in the hexagonal P6₃ space group. This is a non-centrosymmetric structure containing three crystallographic positions of cations: seven-fold coordinated Sr²⁺ (6c) sites, eight-fold coordinated Bi(1) (6c) sites, and eight-fold coordinated Bi(2) (6c) sites. Plenty of crystallographic sites are afforded for doped ions to occupy, thus SrBi₂B₂O₇ is a promising host to prepare phosphor with good luminescence properties. In this work, the new red-emitting borate phosphor SrBi₂B₂O₇:Sm³⁺,Eu³⁺, which has high thermal

^aKey Laboratory of Weak-Light Nonlinear Photonics, Ministry of Education, School of Physics, Nankai University, Tianjin 300071, China. E-mail: lhwu@nankai.edu.cn; Fax: +86-22-23505409; Tel: +86-22-23506257

^bCollege of Electronic Information and Optical Engineering, Tianjin Key Laboratory of Photo-electronic Thin Film Devices and Technology, Nankai University, Tianjin 300071, China. E-mail: yizhang@nankai.edu.cn; Fax: +86-22-23508912; Tel: +86-22-23508572 extn 8018

† Electronic supplementary information (ESI) available: Sm³⁺ and Eu³⁺ codoped SrBi₂B₂O₇: a red-emitting phosphor with improved thermal stability. See DOI: 10.1039/c6ra26752a



stability, is reported for the first time and the high thermal stability mechanism was discussed through defect formation energy calculations. The photoluminescence properties, the energy transfer from Sm^{3+} to Eu^{3+} and the preferred occupancy of the dopant were also investigated in detail.

2. Experimental

2.1 Materials and synthesis

The phosphor samples $\text{SrBi}_2\text{B}_2\text{O}_7:\text{Sm}^{3+}$, $\text{SrBi}_2\text{B}_2\text{O}_7:\text{Eu}^{3+}$, and $\text{SrBi}_2\text{B}_2\text{O}_7:\text{Sm}^{3+}, \text{Eu}^{3+}$ were prepared by high temperature solid-state reaction method. Analytical reagent SrCO_3 , Bi_2O_3 , H_3BO_3 , and high purity (99.99%) Sm_2O_3 and Eu_2O_3 were used as raw materials. These powders were weighed out, well-mixed and ground thoroughly in an agate mortar. The mixtures were first heated at 500 °C for 24 h to decompose the carbonate and eliminate the water. When cooling down to the room temperature, the presintered samples were ground respectively and heated at 650 °C for 72 h, then cooling down to room temperature with the furnace cooling.

2.2 Characterization

X-ray diffraction (XRD) data for phase identification and structural refinement of as-prepared powders were collected by PANalytical powder X-ray diffractometer X'Pert Pro with $\text{Cu K}\alpha$ radiation (40 kV, 40 mA) and the data were collected over a 2θ range from 10° to 140° at an interval of 0.017° with a counting time of 1 s per step. The temperature-dependent XRD patterns were measured on a Rigaku SmartLab X-ray Diffractometer with $\text{Cu K}\alpha$ radiation (40 kV, 180 mA). Those samples to collect XRD data at high temperature are heated from RT to 150 °C with an intermittent heating rate of 3 °C min^{-1} and then kept for 5 min at 150 °C before XRD data collection. High temperature XRD data were collected with a measurement time of 30 min. Photoluminescence (PL), photoluminescence excitation (PLE) spectra were recorded using a spectrofluorometer (Edinburgh Instruments, FLS920) equipped with a Xe light source and double excitation monochromators. Emitted fluorescence was detected by a photomultiplier (R928P) perpendicular to the excitation beam. A cutoff filter was used to eliminate the second-order emission of the source radiation. The luminescence decay was measured by a μF900 lamp (100 W) as a light source and a photomultiplier (R928P) was used as detector. The temperature-dependent luminescence properties were measured on the spectrofluorometer (Edinburgh Instruments, FLS920), combined with a self-made heating attachment (TAP-02). The internal quantum efficiency of optimized-composition phosphors $\text{SrBi}_2\text{B}_2\text{O}_7:0.04\text{Sm}^{3+}$, $\text{SrBi}_2\text{B}_2\text{O}_7:0.06\text{Eu}^{3+}$ and $\text{SrBi}_2\text{B}_2\text{O}_7:0.04\text{Sm}^{3+}, 0.06\text{Eu}^{3+}$ was determined on a standard Edinburgh Instruments FLS920 spectrometer equipped with an integrating sphere attachment.

2.3 Computational details

All the calculations were conducted by first-principles calculations, as implemented in the Vienna *ab initio* simulation package (VASP).^{20,21} The projector augmented wave (PAW) pseudopotential method was used to describe the interactions of

elements. Electronic valence configurations of Sr, Bi, B, O, Sm and Eu were set as $5s^2, 6s^26p^3, 2s^22p^1, 2s^22p^4, 4f^65s^25p^66s^2, 4f^75s^25p^66s^2$, respectively. The exchange–correlation potential used the Perdew–Burke–Ernzerhof (PBE) functional within the spin-polarized generalized gradient approximation (GGA).^{22,23} A plane wave basis with cutoff energy of 400 eV was employed. The k -point sampling for Brillouin zone was generated using a $4 \times 4 \times 2$ -centered grid. In structural optimized process, the energy change, maximum residual force acting on each ion was set as 1×10^{-4} eV per atom, 0.05 eV \AA^{-1} , respectively. As for the formation of defects, they were all obtained through the process that Bi^{3+} ions are replaced equivalently by Sm^{3+} , Eu^{3+} ions or both of them ($\text{Sm}_{\text{Bi}}, \text{Eu}_{\text{Bi}}$) in the conventional cell of $\text{SrBi}_2\text{B}_2\text{O}_7$ whose real stoichiometric formula is $\text{Sr}_6\text{Bi}_{12}\text{B}_{12}\text{O}_{42}$.²⁴ The formation energies of single defect such as Sm_{Bi} as well as Eu_{Bi} and the composite one $\text{Sm}_{\text{Bi}} + \text{Eu}_{\text{Bi}}$ were calculated in our paper.

3. Results and discussion

3.1 Crystal structure

XRD patterns of phosphors $\text{SrBi}_2\text{B}_2\text{O}_7:\text{Sm}^{3+}$, $\text{SrBi}_2\text{B}_2\text{O}_7:\text{Eu}^{3+}$ and $\text{SrBi}_2\text{B}_2\text{O}_7:\text{Sm}^{3+}, \text{Eu}^{3+}$ are shown in Fig. 1. All XRD patterns are found to agree well with that reported in the Inorganic Crystal Structure Database (ICSD #245017), indicating that the doped Sm^{3+} and Eu^{3+} ions do not generate any impurity or induce significant changes in the host structure.

3.2 Luminescence properties of $\text{SrBi}_2\text{B}_2\text{O}_7:\text{Sm}^{3+}, \text{Eu}^{3+}$

The PL and PLE spectra of $\text{SrBi}_2\text{B}_2\text{O}_7:0.04\text{Sm}^{3+}$ are shown in Fig. 2(a). The strongest peak located at 403 nm in the excitation spectrum monitored at 598 nm is attributed to ${}^6\text{H}_{5/2} \rightarrow {}^4\text{F}_{7/2}$ transition. Under the 403 nm excitation, the emission spectra of Sm^{3+} show emission band at 561, 598, 644 and 704 nm due to the ${}^4\text{G}_{5/2} \rightarrow {}^6\text{H}_{J/2}$ ($J = 5, 7, 9, 11$) transitions (red curve in Fig. 2(a)). The quenching concentration of $\text{SrBi}_2\text{B}_2\text{O}_7:\text{Sm}^{3+}$ is 4 mol%, as is

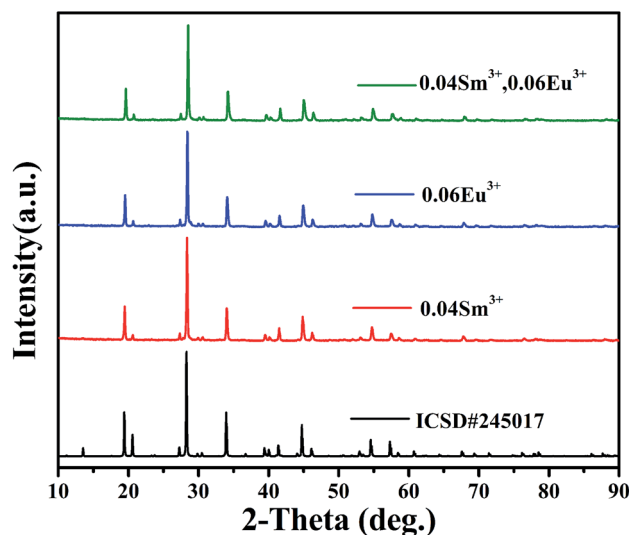


Fig. 1 XRD patterns of $\text{SrBi}_2\text{B}_2\text{O}_7:\text{Sm}^{3+}$, $\text{SrBi}_2\text{B}_2\text{O}_7:\text{Eu}^{3+}$, $\text{SrBi}_2\text{B}_2\text{O}_7:\text{Sm}^{3+}, \text{Eu}^{3+}$ and the ICSD (#245017) of $\text{SrBi}_2\text{B}_2\text{O}_7$.



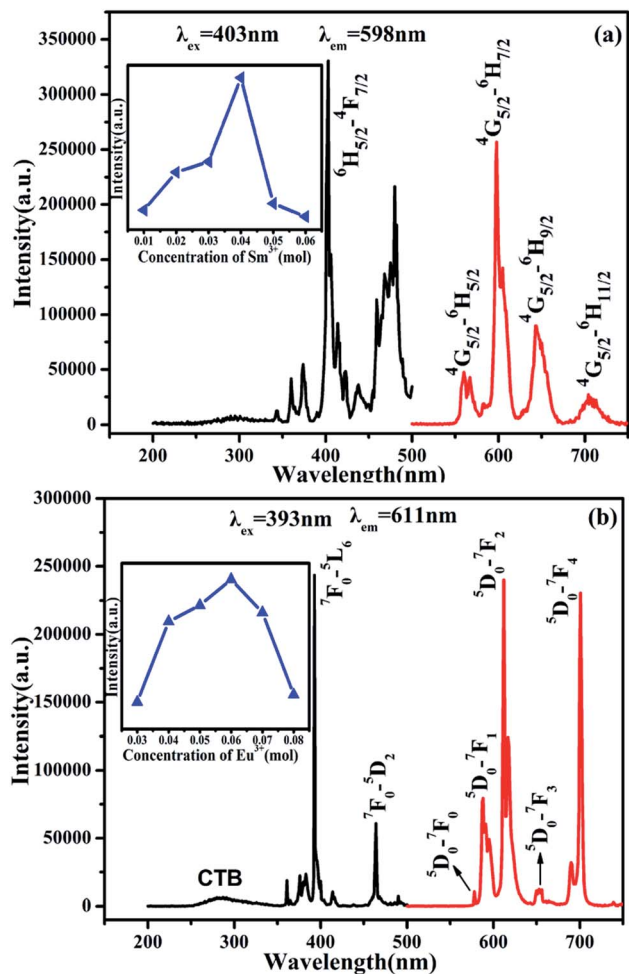


Fig. 2 PL and PLE spectra of SrBi₂B₂O₇:0.04Sm³⁺ (a) and SrBi₂B₂O₇:0.06Eu³⁺ (b). Inset: the dependence of the intensity on Sm³⁺ (a) and Eu³⁺ (b) concentration.

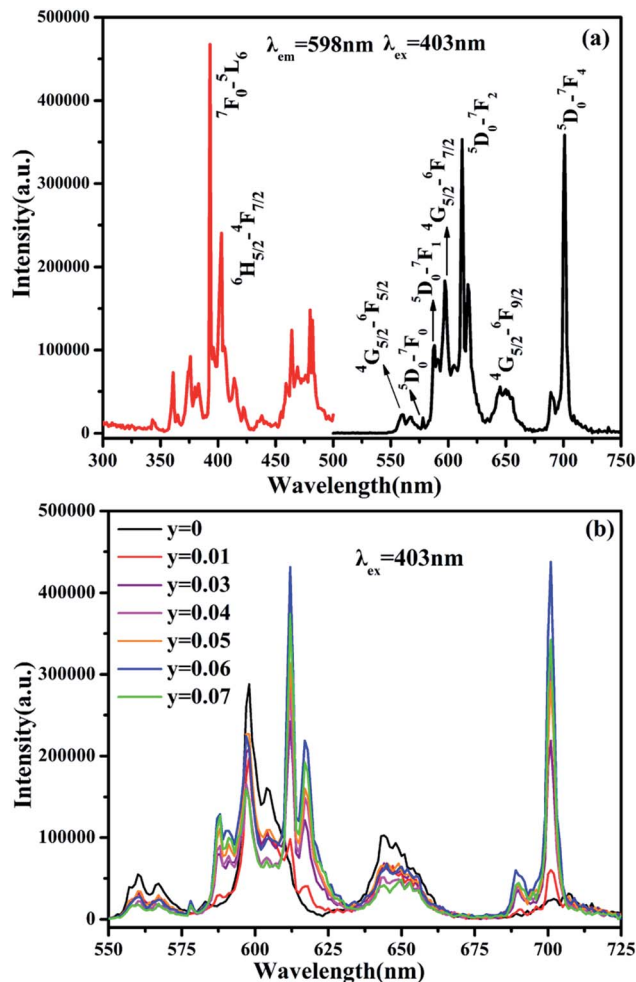


Fig. 3 (a) PLE (left) and PL (right) spectra of SrBi₂B₂O₇:0.04Sm³⁺, 0.06Eu³⁺ phosphor. (b) PL spectra of SrBi₂B₂O₇:0.04Sm³⁺, yEu³⁺ phosphor excited at 403 nm.

shown in the inset of Fig. 2(a). Furthermore, the PL and PLE spectra of SrBi₂B₂O₇:0.06Eu³⁺ are shown in Fig. 2(b). Excited at 393 nm, two main emission bands at 611 nm and 701 nm are attributed to ⁵D₀ → ⁷F₂ and ⁵D₀ → ⁷F₄ transition, and the three weak emission bands of the ⁵D₀ → ⁷F_J (J = 0, 1, 3) are located at around 578 nm, 587 nm and 653 nm. The excitation spectrum consists of the charge transfer band (CTB) and two excitation peaks at 393 and 464 nm, which are mainly caused by the strong f-f transition of ⁷F₀ → ⁵L₆ and ⁷F₀ → ⁵D₂, respectively. The quenching concentration of SrBi₂B₂O₇:Eu³⁺ is 6 mol%, as shown in the inset of Fig. 2(b).

The PL and PLE spectra of Sm³⁺ and Eu³⁺-codoped SrBi₂B₂O₇ phosphor are shown in Fig. 3(a). The PLE spectrum monitored at 598 nm shows two strong excitation peaks at 393 nm and 403 nm, which correspond to the ⁷F₀ → ⁵L₆ transition of Eu³⁺ and ⁶H_{5/2} → ⁴F_{7/2} transition of Sm³⁺, respectively. In the PL spectrum excited at 403 nm, seven significant emission peaks located at 561, 598, 644, 578, 587, 611, 701 nm are observed, which are attributed to ⁴G_{5/2} → ⁶H_{5/2}, ⁴G_{5/2} → ⁶H_{7/2} and ⁴G_{5/2} → ⁶H_{9/2} transition of Sm³⁺ and ⁵D₀ → ⁷F₀, ⁵D₀ → ⁷F₁, ⁵D₀ → ⁷F₂ and ⁵D₀ → ⁷F₄ transition of Eu³⁺, respectively. Fig. 3(b)

shows the PL spectra of SrBi₂B₂O₇:0.04Sm³⁺, yEu³⁺ (y = 0.01–0.07) phosphors excited at 403 nm. All of the characteristic peaks of Sm³⁺ and Eu³⁺ can be observed in the PL spectra of SrBi₂B₂O₇:Sm³⁺, Eu³⁺.

3.3 Thermal stability of SrBi₂B₂O₇:Sm³⁺, Eu³⁺

Thermal stability of the phosphors is very important for the application of w-LEDs, especially for the high-power one. Temperature-dependent PL spectra (excited with λ_{ex} = 403 nm) of SrBi₂B₂O₇:0.04Sm³⁺, 0.06Eu³⁺ at the temperature range of 25–300 °C are shown in Fig. 4(a). Compared to the emission intensity at room temperature, the integrated emission intensities of the characteristic peaks of Sm³⁺ and Eu³⁺ under the excitation of 403 nm at 150 °C were still remained about 87.9% and 83.4% of the initial value, which indicates that the thermal stability of SrBi₂B₂O₇:0.04 Sm³⁺, 0.06Eu³⁺ phosphor is good. The temperature dependent PL spectra of Sm³⁺ doped SrBi₂B₂O₇ and Eu³⁺ doped SrBi₂B₂O₇ were also measured. Fig. 4(b) is the normalized PL intensities of SrBi₂B₂O₇:Sm³⁺, Eu³⁺, SrBi₂B₂O₇:Sm³⁺, and SrBi₂B₂O₇:Eu³⁺. The PL intensities of the commercial



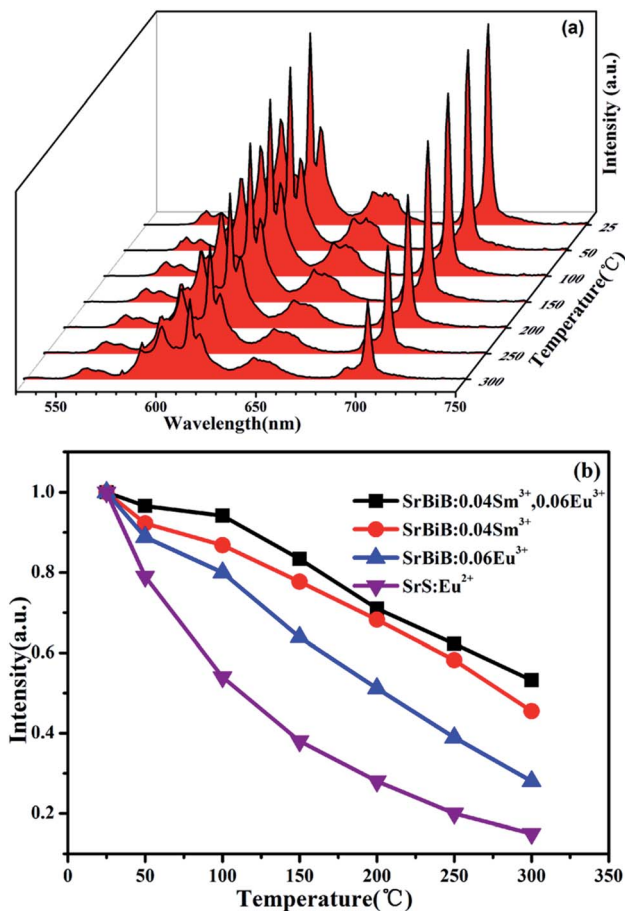


Fig. 4 (a) Temperature-dependent PL spectra of $\text{SrBi}_2\text{B}_2\text{O}_7:0.04\text{Sm}^{3+}, 0.06\text{Eu}^{3+}$ phosphor ($\lambda_{\text{ex}} = 403 \text{ nm}$). (b) The comparison results of PL intensities of $\text{SrBi}_2\text{B}_2\text{O}_7$ (SrBiB): $0.04\text{Sm}^{3+}, 0.06\text{Eu}^{3+}$ ($\lambda_{\text{ex}} = 403 \text{ nm}$), $\text{SrBi}_2\text{B}_2\text{O}_7:0.04\text{Sm}^{3+}$ ($\lambda_{\text{ex}} = 403 \text{ nm}$), $\text{SrBi}_2\text{B}_2\text{O}_7:0.06\text{Eu}^{3+}$ ($\lambda_{\text{ex}} = 393 \text{ nm}$) as a function of temperature. As a comparison, thermal quenching data of $\text{SrS}:\text{Eu}^{2+}$ excited at 460 nm are also measured.

red phosphor $\text{SrS}:\text{Eu}^{2+}$ is also shown in Fig. 4(b). It is very interesting that the thermal stability of Sm^{3+} and Eu^{3+} codoped phosphor is better than those of $\text{Sm}^{3+}/\text{Eu}^{3+}$ single doped phosphors, which are all superior to that of $\text{SrS}:\text{Eu}^{2+}$.

Why the thermal stability is enhanced as Sm^{3+} and Eu^{3+} codoped into the $\text{SrBi}_2\text{B}_2\text{O}_7$? Up to date, the mechanism of high thermal stability enhanced by rare ions codoping is rarely investigated.

To clarify this question, we first study the local crystal environment of Sm^{3+} and Eu^{3+} in $\text{SrBi}_2\text{B}_2\text{O}_7$. The host $\text{SrBi}_2\text{B}_2\text{O}_7$ crystallizes in the hexagonal space group $P6_3$ with $a = 9.1404(4) \text{ \AA}$, $c = 13.0808(6) \text{ \AA}$, $V = 946.44(7) \text{ \AA}^3$ and $Z = 6$. In the non-centrosymmetric structure, the Bi atoms are weakly bonded to the O atoms with strongly asymmetric eight-fold coordination environment.

The BiO_8 coordination polyhedra and alternating BO_3 triangles are in one layer and linked by edge-sharings, while Sr atoms are in the adjacent layer, as is shown in Fig. 5. There are three crystallographic positions of cations in the unit cell: seven-fold coordinated Sr^{2+} (6c) sites, eight-fold coordinated Bi(1) (6c) sites, and

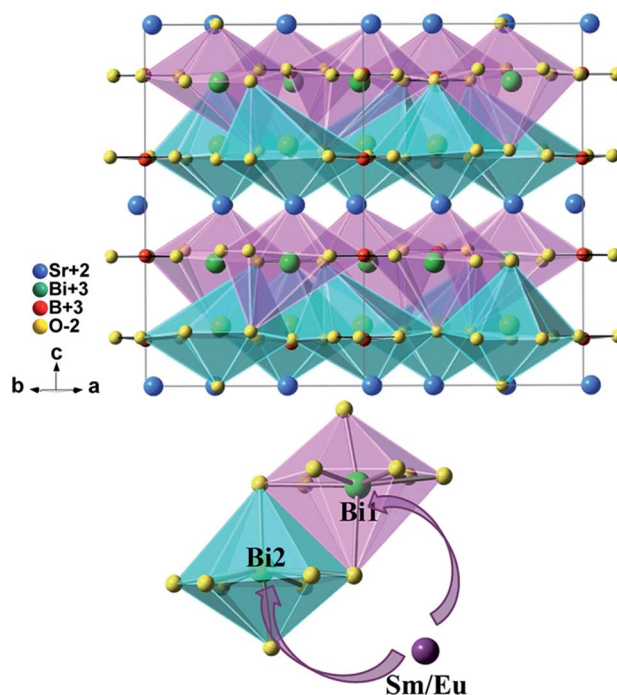


Fig. 5 Crystal structure of $\text{SrBi}_2\text{B}_2\text{O}_7$ and site occupancy preference of $\text{Sm}^{3+}/\text{Eu}^{3+}$ ions to Bi1 and Bi2 in $\text{SrBi}_2\text{B}_2\text{O}_7$.

eight-fold coordinated Bi(2) (6c) sites. As reported by Shannon,²⁵ the effective ionic radius (r) of Sm^{3+} , Eu^{3+} and Bi^{3+} is 1.08 \AA , 1.07 \AA and 1.17 \AA , respectively as the coordination number (CN) equals 8, whereas $r_{\text{Sm}^{3+}} = 1.02 \text{ \AA}$, $r_{\text{Eu}^{3+}} = 1.01 \text{ \AA}$ and $r_{\text{Sr}^{2+}} = 1.21 \text{ \AA}$ as CN = 7. Considering the r and CN, it seems that all the three sites can be occupied by Sm^{3+} and Eu^{3+} .

To clarify the structure and the local crystal environment of Sm^{3+} and Eu^{3+} in $\text{SrBi}_2\text{B}_2\text{O}_7$, the refinement on the XRD patterns of $\text{SrBi}_{1.96}\text{Sm}_{0.04}\text{B}_2\text{O}_7$, $\text{SrBi}_{1.94}\text{Eu}_{0.06}\text{B}_2\text{O}_7$, and $\text{SrBi}_{1.90}\text{Sm}_{0.04}\text{Eu}_{0.06}\text{B}_2\text{O}_7$ are performed by Rietveld method^{26,27} within the Fullprof Program.²⁸ The final agreement factors converged to $R_p = 8.50\%$, $R_{\text{wp}} = 9.60\%$, and $R_{\text{exp}} = 3.90\%$ for $\text{SrBi}_{1.96}\text{Sm}_{0.04}\text{B}_2\text{O}_7$, $R_p = 7.40\%$, $R_{\text{wp}} = 9.79\%$, and $R_{\text{exp}} = 4.03\%$ for $\text{SrBi}_{1.94}\text{Eu}_{0.06}\text{B}_2\text{O}_7$, and $R_p = 7.39\%$, $R_{\text{wp}} = 9.64\%$, and $R_{\text{exp}} = 3.97\%$ for $\text{SrBi}_{1.90}\text{Sm}_{0.04}\text{Eu}_{0.06}\text{B}_2\text{O}_7$. Lattice parameters are refined to $a = 9.1215(2) \text{ \AA}$, $c = 13.0550(9) \text{ \AA}$, and $V = 940.67(4) \text{ \AA}^3$ for $\text{SrBi}_{1.96}\text{Sm}_{0.04}\text{B}_2\text{O}_7$; $a = 9.1128(3) \text{ \AA}$, $c = 13.0492(5) \text{ \AA}$, and $V = 938.47(6) \text{ \AA}^3$ for $\text{SrBi}_{1.94}\text{Eu}_{0.06}\text{B}_2\text{O}_7$; $a = 9.1084(7) \text{ \AA}$, $c = 13.0452(6) \text{ \AA}$, and $V = 937.28(6) \text{ \AA}^3$ for $\text{SrBi}_{1.90}\text{Sm}_{0.04}\text{Eu}_{0.06}\text{B}_2\text{O}_7$.

Fig. 5 shows the crystal structure of $\text{SrBi}_2\text{B}_2\text{O}_7$. The final refinement patterns are given in Fig. 6. The crystallographic data, fractional atomic coordinates and occupancy are listed in Tables 1 and S1.†

The final compositions determined by refinements are in good agreement with the nominal composition of the starting materials, as shown in Table S1.† It can be seen that the doped cations are preferred to occupy the Bi(1) (6c) sites and Bi(2) (6c) sites simultaneously for all of the $\text{Sm}^{3+}/\text{Eu}^{3+}$ single doped samples or codoped samples. This site occupancy is quite different from that of $\text{ZnBi}_2\text{B}_2\text{O}_7:\text{Eu}^{3+}$,⁶ in which the Eu^{3+} ions



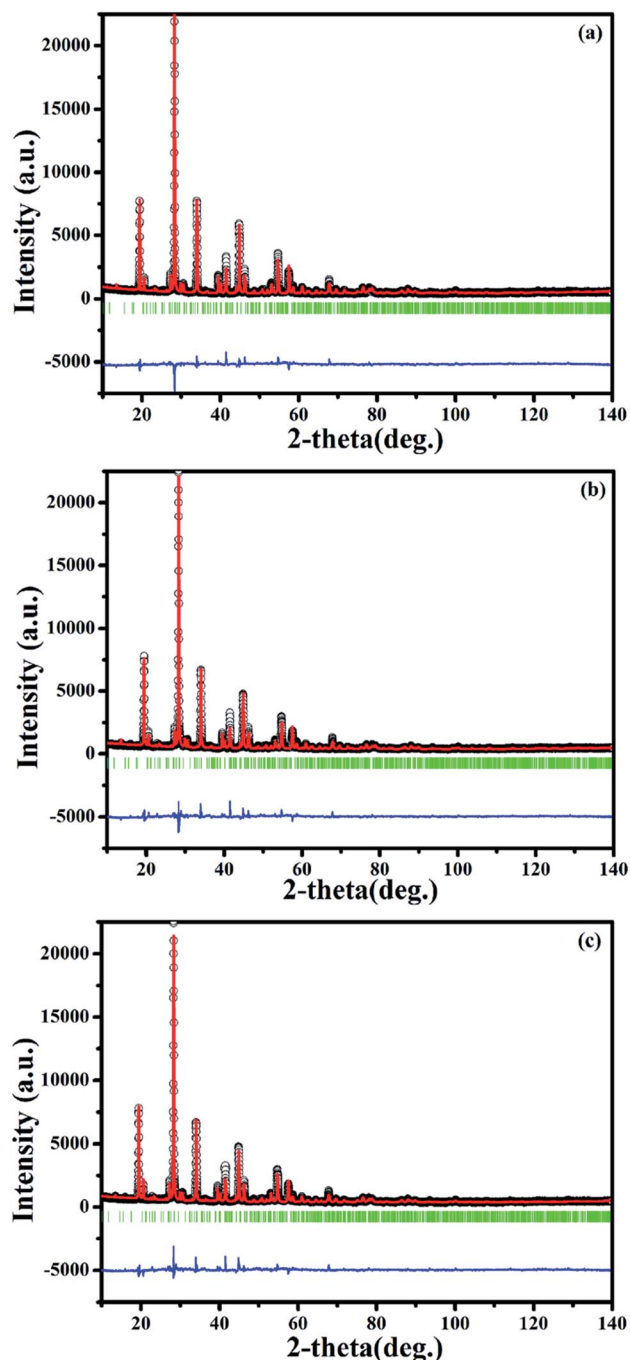


Fig. 6 Final Rietveld refinement of the XRD profiles of SrBi_{1.96}Sm_{0.04}B₂O₇ (a), SrBi_{1.94}Eu_{0.06}B₂O₇ (b) and SrBi_{1.90}Sm_{0.04}Eu_{0.06}B₂O₇ (c) at room temperature. Small black circles and the red continuous lines represent the experimental and the calculated values respectively; vertical bars (|) indicate the position of Bragg peaks. The blue bottom trace depicts the corresponding residuals between the experimental and the calculated intensity values.

are preferred to only occupy the Zn site instead of Bi sites. ZnBi₂B₂O₇ and SrBi₂B₂O₇ are nearly the same in the chemical formula. However, their structures are different. ZnBi₂B₂O₇ adopts an orthorhombic structure with space group *Pba2* and *Z* = 4. The Bi³⁺ cations in ZnBi₂B₂O₇ occupy two distinct interlayer sites with asymmetric six-fold coordination environments. The

Table 1 Crystallographic data and Rietveld refinement data for SrBi_{2-x-y}Sm_xEu_yB₂O₇ at room temperature

Chemical formula	<i>x</i> = 0.04, <i>y</i> = 0	<i>x</i> = 0, <i>y</i> = 0.06	<i>x</i> = 0.04, <i>y</i> = 0.06
Crystal system	Hexagonal	Hexagonal	Hexagonal
Space group	<i>P6</i> ₃	<i>P6</i> ₃	<i>P6</i> ₃
<i>a</i> /Å	9.1215(2)	9.1128(3)	9.1084(7)
<i>c</i> /Å	13.0550(9)	13.0492(5)	13.0452(6)
<i>V</i> /Å ³	940.67(4)	938.47(6)	937.28(6)
<i>Z</i>	6	6	6
<i>R</i> _p (%)	8.50	7.40	7.39
<i>R</i> _{wp} (%)	9.60	9.79	9.64
<i>R</i> _{exp} (%)	3.90	4.03	3.97
<i>R</i> _{Bragg} (%)	8.61	9.52	9.86

bond valence sum for Bi(1) and Bi(2) in ZnBi₂B₂O₇ is 2.93 and 2.99, respectively,²⁹ which is close to the theoretical value of 3. However, the Bi³⁺ cations and O²⁻ anions are weakly bonded in SrBi₂B₂O₇. The weak bonding interactions can result in the fragility and easy cleavage. The bond valence sum for Bi(1) and Bi(2) in SrBi₂B₂O₇ is 2.39 and 2.29, respectively,¹⁹ which is much lower than those in ZnBi₂B₂O₇ and indicates a significant underbonding. Thus, the Bi³⁺ cations in SrBi₂B₂O₇ are much more unstable than that in ZnBi₂B₂O₇. Then the different occupancy preferences of the dopants are observed in ZnBi₂B₂O₇ and SrBi₂B₂O₇.

On this basis, the refinement on the XRD patterns of SrBi_{1.96}Sm_{0.04}B₂O₇, SrBi_{1.94}Eu_{0.06}B₂O₇ and SrBi_{1.90}Sm_{0.04}Eu_{0.06}B₂O₇ at 150 °C are further performed by Rietveld refinement within the Fullprof Program to clarify the change of the local crystal environment of Sm³⁺ and Eu³⁺ in SrBi₂B₂O₇. The final agreement factors converged to *R*_p = 7.91%, *R*_{wp} = 12.10% and *R*_{exp} = 3.96% for SrBi_{1.96}Sm_{0.04}B₂O₇, *R*_p = 8.90%, *R*_{wp} = 12.90% and *R*_{exp} = 4.03% for SrBi_{1.94}Eu_{0.06}B₂O₇, and *R*_p = 9.06%, *R*_{wp} = 13.10% and *R*_{exp} = 3.97% for SrBi_{1.90}Sm_{0.04}Eu_{0.06}B₂O₇. Lattice parameters are refined to *a* = 9.1194(3) Å, *c* = 13.0520(4) Å, and *V* = 940.02(5) Å³ for SrBi_{1.96}Sm_{0.04}B₂O₇, *a* = 9.1100(3) Å, *c* = 13.0440(5) Å, and *V* = 937.51(5) Å³ for SrBi_{1.94}Eu_{0.06}B₂O₇, and *a* = 9.1057(3) Å, *c* = 13.0406(5) Å, and *V* = 936.40(6) Å³ for SrBi_{1.90}Sm_{0.04}Eu_{0.06}B₂O₇. The final refinement patterns are given in Fig. 7. The crystallographic data, fractional atomic coordinates and occupancy are listed in Tables 2 and S2;† selected average bond lengths (Å) of Bi–O are reported in Table S3.†

As comparing the refined lattice parameters at 150 °C with those at room temperature, it is very interesting that the lattice parameters *a*, *c*, and *V* become smaller for both codoped and single doped samples. This unusual phenomenon is contrary to the rule of thermal expansion and contraction. Furthermore, as indicated in Table S3,† for the codoped and single doped phosphors, the average bond lengths between Bi (6c) and O (6c) sites at 150 °C is shorter than that at room temperature. Also, the average bond lengths of Bi–O in codoped phosphors at high temperature or RT is shorter than those in single doped phosphors at the same temperature. The above results indicates that the crystal structure of the codoped and single doped phosphors at high temperature is more compact than those of the



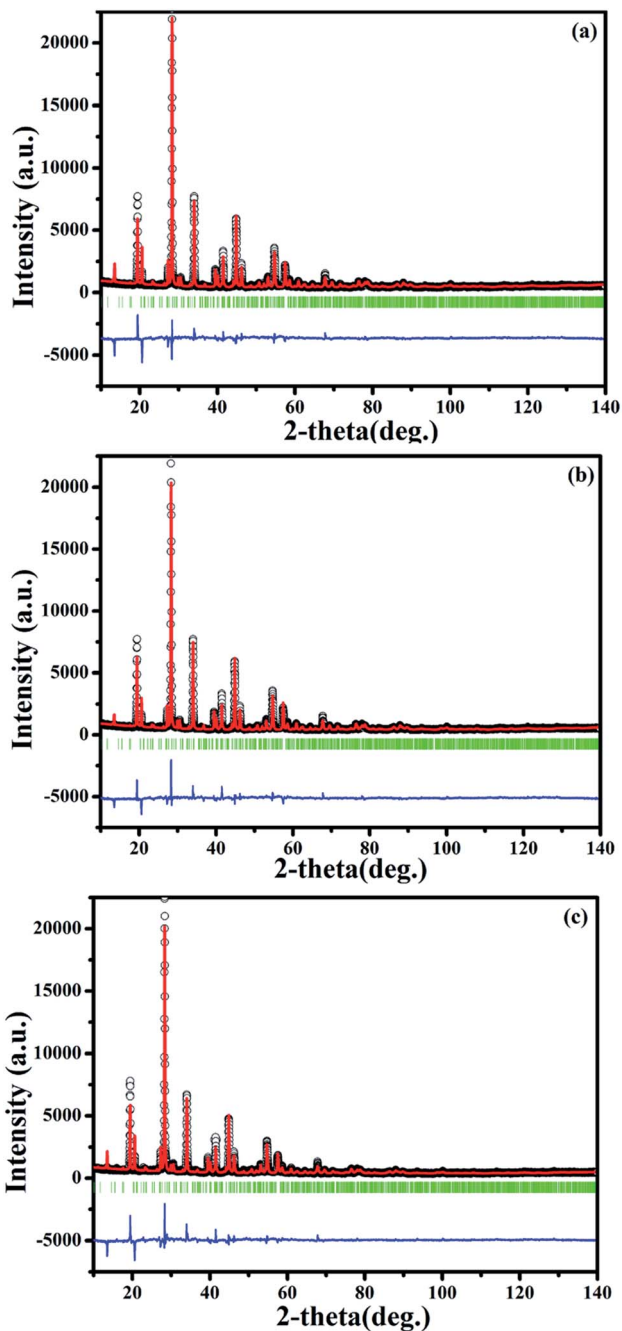


Fig. 7 Final Rietveld refinement of the XRD profiles of $\text{SrBi}_{1.96}\text{Sm}_{0.04}\text{B}_2\text{O}_7$ (a), $\text{SrBi}_{1.94}\text{Eu}_{0.06}\text{B}_2\text{O}_7$ (b) and $\text{SrBi}_{1.90}\text{Sm}_{0.04}\text{Eu}_{0.06}\text{B}_2\text{O}_7$ (c) at 150 °C.

phosphors at room temperature, which should contribute to the improved thermal stability as Sm^{3+} and Eu^{3+} codoped into $\text{SrBi}_2\text{B}_2\text{O}_7$.

In addition, to investigate whether the high thermal stability is related with the electronic band gap, the electronic band structures of $\text{Sm}^{3+}/\text{Eu}^{3+}$ singledoped $\text{SrBi}_2\text{B}_2\text{O}_7$, Sm^{3+} and Eu^{3+} codoped $\text{SrBi}_2\text{B}_2\text{O}_7$ and undoped $\text{SrBi}_2\text{B}_2\text{O}_7$ are computed with VASP and shown in Fig. 8. The electronic band gap of $\text{SrBi}_2\text{B}_2\text{O}_7:\text{Eu}^{3+}$, $\text{SrBi}_2\text{B}_2\text{O}_7:\text{Sm}^{3+}$, $\text{SrBi}_2\text{B}_2\text{O}_7:\text{Sm}^{3+}$, Eu^{3+} and $\text{SrBi}_2\text{B}_2\text{O}_7$ are 2.57, 2.78, 2.60 and 2.81 eV, respectively. They are different

Table 2 Crystallographic data and Rietveld refinement data for $\text{SrBi}_{2-x-y}\text{Sm}_x\text{Eu}_y\text{B}_2\text{O}_7$ at 150 °C

Chemical formula	$x = 0.04$, $y = 0$	$x = 0$, $y = 0.06$	$x = 0.04$, $y = 0.06$
Crystal system	Hexagonal	Hexagonal	Hexagonal
Space group	$P6_3$	$P6_3$	$P6_3$
$a/\text{Å}$	9.1194(3)	9.1100(3)	9.1057(3)
$c/\text{Å}$	13.0520(4)	13.0440(5)	13.0406(5)
$V/\text{Å}^3$	940.02(5)	937.51(5)	936.40(6)
Z	6	6	6
R_p (%)	7.91	8.90	9.06
R_{wp} (%)	12.10	12.90	13.10
R_{exp} (%)	3.96	4.03	3.97
R_{Bragg} (%)	9.87	10.10	10.35

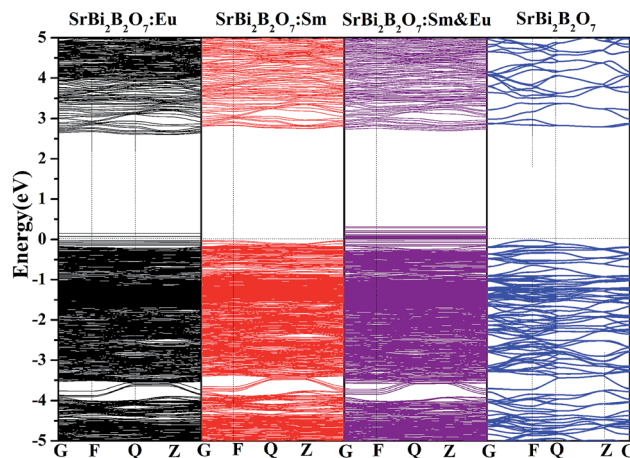


Fig. 8 Electronic band structures of undoped and doped $\text{SrBi}_2\text{B}_2\text{O}_7$. The Fermi level is set to 0 eV.

somewhat. However, the difference among these electronic band gaps are small, which means that the electronic band structure should not be the main reason to enhance the thermal stability as Sm^{3+} and Eu^{3+} codoped into $\text{SrBi}_2\text{B}_2\text{O}_7$.

As rare earth ions doped into the host, the corresponding defects will be formed. As studied on the site occupancy of the doped ions in this study, Sm^{3+} and Eu^{3+} ions are preferred to occupy Bi sites, thus the formed defects should mainly be Sm_{Bi} and Eu_{Bi} . For the formed defects, the defect formation energy (E_f) will be different because of the different doped ions. In this study, to clarify the difference of E_f among Sm^{3+} , Eu^{3+} single doped and codoped $\text{SrBi}_2\text{B}_2\text{O}_7$, E_f of $\text{SrBi}_{1.90}\text{Sm}_{0.04}\text{Eu}_{0.06}\text{B}_2\text{O}_7$, $\text{SrBi}_{1.94}\text{Sm}_{0.06}\text{B}_2\text{O}_7$ and $\text{SrBi}_{1.96}\text{Eu}_{0.04}\text{B}_2\text{O}_7$ defined as the following formula,^{30,31} are calculated with VASP.

$$E_f = E(\text{Sr}_6\text{Bi}_{12-x-y}\text{B}_{12}\text{O}_{42}\text{Sm}_x\text{Eu}_y) - E(\text{Sr}_6\text{Bi}_{12}\text{B}_{12}\text{O}_{42}) - x\mu_{\text{Sm}} - y\mu_{\text{Eu}} + (x+y)\mu_{\text{Bi}} \quad (1)$$

where $E(\text{Sr}_6\text{Bi}_{12-x-y}\text{B}_{12}\text{O}_{42}\text{Sm}_x\text{Eu}_y)$ and $E(\text{Sr}_6\text{Bi}_{12}\text{B}_{12}\text{O}_{42})$ are the total energy of the rare earth doped compound and pure compound, respectively. μ_{Sm} , μ_{Eu} and μ_{Bi} are the chemical potentials of bulk Sm, Eu and Bi, respectively. The total energy (E_{tot}) and defect formation energy (E_f) of the $\text{Sr}(\text{Bi},\text{M})_2\text{B}_2\text{O}_7$ ($\text{M} =$



Table 3 Total energy (E_{tot}) and formation energy (E_f) of the Sr(Bi,M) $_2$ B $_2$ O $_7$ (M = Sm, Eu)

Sample compositions	E_{tot} (eV)	E_f (eV)
SrBi $_{1.90}$ Sm $_{0.04}$ Eu $_{0.06}$ B $_2$ O $_7$	-530.84	-5.47
SrBi $_{1.94}$ Sm $_{0.06}$ B $_2$ O $_7$	-517.67	-5.20
SrBi $_{1.96}$ Eu $_{0.04}$ B $_2$ O $_7$	-510.15	0.30

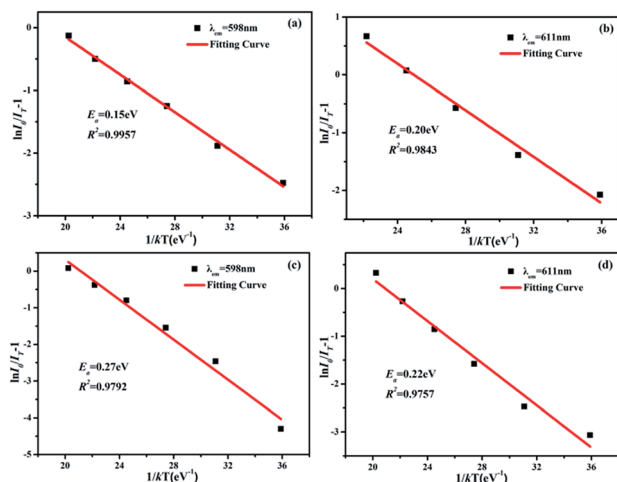


Fig. 9 The $\ln(I_0/I_T - 1)$ vs. $1/KT$ activation energy graph for thermal quenching of the characteristic emission of Sm $^{3+}$ (a) in SrBi $_2$ B $_2$ O $_7$:0.04Sm $^{3+}$ phosphor, Eu $^{3+}$ (b) in SrBi $_2$ B $_2$ O $_7$:0.06Eu $^{3+}$ phosphor, Sm $^{3+}$ (c) and Eu $^{3+}$ (d) in SrBi $_2$ B $_2$ O $_7$:0.04Sm $^{3+}$,0.06Eu $^{3+}$ phosphor.

Sm, Eu) are listed in Table 3, in which case A, B, C represents SrBi $_{1.90}$ Sm $_{0.04}$ Eu $_{0.06}$ B $_2$ O $_7$, SrBi $_{1.94}$ Sm $_{0.06}$ B $_2$ O $_7$ and SrBi $_{1.96}$ Eu $_{0.04}$ B $_2$ O $_7$, respectively. It is indicated that the defect formation energy of the case A (*i.e.* Sm $^{3+}$ and Eu $^{3+}$ codoped sample) is -5.47 eV, which is the lowest value among case A, B and C (the defect formation energies of case B and case C are -5.20 eV and 0.30 eV, respectively). The defect formation energies of Sm $^{3+}$ and Eu $^{3+}$ co-doped and Sm $^{3+}$ single doped phosphors are ~5.77 eV and ~5.50 eV lower than that of Eu $^{3+}$ single doped phosphor, respectively. These big obvious energy differences indicate that it is much easier to form the double defects like Sm $_{\text{Bi}}$ and Eu $_{\text{Bi}}$ than single ones. For the single defect, Sm $_{\text{Bi}}$ is much easier to form than Eu $_{\text{Bi}}$. From the total energy of the case A, B, and C, they also have the same trend as formation energy. Thus, as the phosphors were heated to high temperature, the double defects like Sm $_{\text{Bi}}$ and Eu $_{\text{Bi}}$ will be more stable than the single ones. So the improvement of thermal stability of Sm $^{3+}$ and Eu $^{3+}$ codoped into SrBi $_2$ B $_2$ O $_7$ should mainly because of the large defect formation energy of double defects.

The active energy of Sm $^{3+}$ and Eu $^{3+}$ codoped SrBi $_2$ B $_2$ O $_7$ phosphor was also studied. It is well known that the decrease of the emission intensity at different temperature can be described by the Arrhenius equation:³²

$$I_T = I_0/[1 + \exp(-E_a/kT)] \quad (2)$$

where I_0 and I_T are the luminescence intensities of SrBi $_2$ B $_2$ O $_7$:0.04Sm $^{3+}$,0.06Eu $^{3+}$ at room temperature and the testing temperature, respectively. E_a is the activation energy and k is the Boltzmann constant (8.617×10^{-5} eV K $^{-1}$). As is displayed in Fig. 9, E_a of Sm $^{3+}$ and Eu $^{3+}$ in SrBi $_2$ B $_2$ O $_7$:Sm $^{3+}$, Eu $^{3+}$ obtained to be 0.27 eV and 0.22 eV are bigger than the E_a of Sm $^{3+}$ in SrBi $_2$ B $_2$ O $_7$:Sm $^{3+}$ and Eu $^{3+}$ in SrBi $_2$ B $_2$ O $_7$:Eu $^{3+}$, which are calculated to be 0.15 eV and 0.20 eV, respectively. These results further indicate that the Sm $^{3+}$ and Eu $^{3+}$ codoped phosphor has good thermal stability.

3.4 Quantum efficiency

Quantum efficiency is an important parameter for LED phosphor. To determine the absolute quantum efficiency of photo-conversion for the SrBi $_2$ B $_2$ O $_7$:Sm $^{3+}$, Eu $^{3+}$ phosphor, the optical absorbance (A) and internal quantum efficiency (η_{int}) was measured using the integrated sphere method. The absorbance can be calculated according to the equation:

$$A = \frac{L_0(\lambda) - L_i(\lambda)}{L_0(\lambda)} \quad (3)$$

where $L_0(\lambda)$ is the integrated excitation profile when the sample is diffusely illuminated by the integrated sphere's surface and $L_i(\lambda)$ is the integrated excitation profile when the sample is directly excited by the incident beam. Furthermore, the internal quantum efficiency (QE) of the phosphors can be calculated by.

$$\eta_{\text{int}} = \frac{E_i(\lambda) - (1 - A)E_0(\lambda)}{L_e(\lambda)A} \quad (4)$$

where $E_i(\lambda)$ is the integrated luminescence of the powder upon direct excitation, and $E_0(\lambda)$ is the integrated luminescence of the powder excited by indirect illumination from the sphere. The term $L_e(\lambda)$ is the integrated excitation profile obtained from the empty integrated sphere (without the sample present). The internal quantum efficiency (QE) of the SrBi $_2$ B $_2$ O $_7$:0.04Sm $^{3+}$ phosphor and SrBi $_2$ B $_2$ O $_7$:0.04Sm $^{3+}$,0.06Eu $^{3+}$ phosphor both under 403 nm excitation, SrBi $_2$ B $_2$ O $_7$:0.06Eu $^{3+}$ phosphor excited at 393 nm are determined to be 33.2%, 42.6%, and 37.5% respectively, indicating the Sm $^{3+}$ and Eu $^{3+}$ codoped phosphor has better internal QE.

4. Conclusions

In conclusion, a red-emitting SrBi $_2$ B $_2$ O $_7$:Sm $^{3+}$,Eu $^{3+}$ phosphor with improved thermal stability was synthesized through solid state reactions. The origin of the reason why thermal stability is improved is studied. The structural study results indicate that the doped Sm $^{3+}$ and Eu $^{3+}$ ions are inclined to occupy Bi(1) (6c) and Bi(2) (6c) sites simultaneously and the crystal structure of the SrBi $_2$ B $_2$ O $_7$:Sm $^{3+}$, Eu $^{3+}$ was more compact at high temperature than that at room temperature. According to the first-principles calculation, the lowest defect formation energy -5.47 eV is obtained in the Sm $^{3+}$ and Eu $^{3+}$ codoped SrBi $_2$ B $_2$ O $_7$ phosphor, which discloses that the defect formation energy should be another intrinsically responsible for the thermal



stable luminescence of red-emitting SrBi₂B₂O₇:Sm³⁺, Eu³⁺ phosphor.

Acknowledgements

This work was financially supported by National Natural Science Foundation of China (51372121, 61274053, U1460201, 51572132), Natural Science Foundation of Tianjin (14JCYBJC17800) and 111 Project (No. B07013) and YangFan Innovative & Entrepreneurial Research Team Project (2014YT02N037). We thank Mrs Xu of A02 group, Institute of Physics, Chinese Academy of Science for her great help in collecting the powder X-ray diffraction data.

References

- 1 R. J. Xie, N. Hirosaki, N. Kimura, K. Sakuma and M. Mitomo, *Appl. Phys. Lett.*, 2007, **90**, 191101.
- 2 Y. Q. Li, J. E. J. Van Steen, J. W. H. Van Krevel, G. Botty, A. C. A. Delsing, F. J. Disalvo, G. De With and H. T. Hintzen, *J. Alloys Compd.*, 2007, **417**, 273.
- 3 J. Xu, Z. H. Ju, X. P. Gao, Y. Q. An, X. L. Tang and W. S. Liu, *Inorg. Chem.*, 2013, **52**, 13875.
- 4 S. Kamimura, H. Yamada and C. N. Xu, *Appl. Phys. Lett.*, 2012, **101**, 091113.
- 5 C. C. Lin, Z. R. Xiao, G. Y. Guo, T. S. Chan and R. S. Liu, *J. Am. Chem. Soc.*, 2010, **132**, 3020.
- 6 L. W. Wu, F. X. Zhang, L. Wu, H. Yi, H. R. Wang and Y. Zhang, *J. Alloys Compd.*, 2015, **648**, 500.
- 7 H. Yi, F. Li, L. Wu, L. W. Wu, H. R. Wang, B. Wang, Y. Zhang, Y. F. Kong and J. J. Xu, *RSC Adv.*, 2014, **6**, 64244.
- 8 Y. Zhang, L. Wu, M. Y. Ji, B. Wang, Y. F. Kong and J. J. Xu, *Opt. Mater. Express*, 2012, **1**, 92.
- 9 Y. L. Huang, Y. Nakai, T. Tsuboi and H. J. Seo, *Opt. Express*, 2011, **19**, 6303.
- 10 J. G. Li, X. D. Li, X. D. Sun and T. Ishigaki, *J. Phys. Chem. C*, 2008, **112**, 11707.
- 11 Z. G. Xia and D. M. Chen, *J. Am. Ceram. Soc.*, 2010, **93**, 1397.
- 12 L. L. Wang, H. M. Noh, B. K. Moon, S. H. Park, K. H. Kim, J. Shi and J. H. Jeong, *J. Phys. Chem. C*, 2015, **119**, 15517.
- 13 W. R. Liu, C. H. Huang, C. P. Wu, Y. C. Chiu, Y. T. Yeh and T. M. Chen, *J. Mater. Chem.*, 2011, **21**, 6869.
- 14 Z. G. Xia, J. Q. Zhuang and L. B. Liao, *Inorg. Chem.*, 2012, **51**, 7202.
- 15 L. Wu, M. Y. Ji, H. R. Wang, Y. F. Kong and Y. Zhang, *Opt. Mater. Express*, 2014, **8**, 1535.
- 16 D. Kang, H. S. Yoo, S. H. Jung, H. Kim and D. Y. Jeon, *J. Phys. Chem. C*, 2011, **115**, 24334.
- 17 X. Min, Z. H. Huang, M. H. Fang, Y. G. Liu, C. Tang and X. W. Wu, *Inorg. Chem.*, 2014, **53**, 6060.
- 18 J. H. Chen, W. R. Zhao, J. Q. Wang, N. H. Wang, Y. J. Meng, J. He and X. Zhang, *Ceram. Int.*, 2015, **41**, 11945.
- 19 J. Barbier and L. M. D. Cranswick, *J. Solid State Chem.*, 2006, **179**, 3958.
- 20 G. Kresse and J. Hafner, *Phys. Rev. B: Condens. Matter Mater. Phys.*, 1993, **47**, 558.
- 21 G. Kresse and J. Furthmüller, *Phys. Rev. B: Condens. Matter Mater. Phys.*, 1996, **54**, 11169.
- 22 J. P. Perdew, K. Burke and M. Ernzerhof, *Phys. Rev. Lett.*, 1996, **77**, 3865.
- 23 H. J. Monkhorst and J. D. Pack, *Phys. Rev. B: Solid State*, 1976, **13**, 5188.
- 24 B. Y. Qu, B. Zhang, L. Wang, R. L. Zhou and X. C. Zeng, *Chem. Mater.*, 2015, **27**, 2195.
- 25 R. Shannon, *Acta Crystallogr., Sect. A: Cryst. Phys., Diffraction, Theor. Gen. Crystallogr.*, 1976, **32**, 751.
- 26 H. M. Rietveld, *Acta Crystallogr.*, 1967, **22**, 151.
- 27 H. M. Rietveld, *J. Appl. Crystallogr.*, 1969, **2**, 65.
- 28 J. Rodriguez-Carvajal, M. T. Fernandez-Diaz and J. L. Martinez, *J. Phys.: Condens. Matter*, 1991, **3**, 3215.
- 29 J. Barbier, N. Penin and L. M. D. Cranswick, *Chem. Mater.*, 2005, **17**, 3130.
- 30 A. F. Kohan, G. Ceder, D. Morgan and C. G. Van de Walle, *Phys. Rev. B: Condens. Matter Mater. Phys.*, 2000, **61**, 15019.
- 31 B. Liu, M. Gu and X. L. Liu, *Appl. Phys. Lett.*, 2010, **97**, 122101.
- 32 H. Jing, C. F. Guo, G. G. Zhang, X. Y. Su, Z. Yang and J. H. Jeong, *J. Mater. Chem.*, 2012, **22**, 13612.

